frontiers in Microbiology

ORIGINAL RESEARCH
published: 24 September 2021
doi: 10.3389/fmicb.2021.747905

Force and Stepwise Movements of Gliding Motility in Human Pathogenic Bacterium *Mycoplasma pneumoniae*

Masaki Mizutani[1†], Yuya Sasajima[1] and Makoto Miyata[1,2*]

[1] Graduate School of Science, Osaka City University, Osaka, Japan, [2] The OCU Advanced Research Institute for Natural Science and Technology (OCARINA), Osaka City University, Osaka, Japan

Mycoplasma pneumoniae, a human pathogenic bacterium, binds to sialylated oligosaccharides and glides on host cell surfaces *via* a unique mechanism. Gliding motility is essential for initiating the infectious process. In the present study, we measured the stall force of an *M. pneumoniae* cell carrying a bead that was manipulated using optical tweezers on two strains. The stall forces of M129 and FH strains were averaged to be 23.7 and 19.7 pN, respectively, much weaker than those of other bacterial surface motilities. The binding activity and gliding speed of the M129 strain on sialylated oligosaccharides were eight and two times higher than those of the FH strain, respectively, showing that binding activity is not linked to gliding force. Gliding speed decreased when cell binding was reduced by addition of free sialylated oligosaccharides, indicating the existence of a drag force during gliding. We detected stepwise movements, likely caused by a single leg under 0.2-0.3 mM free sialylated oligosaccharides. A step size of 14-19 nm showed that 25-35 propulsion steps per second are required to achieve the usual gliding speed. The step size was reduced to less than half with the load applied using optical tweezers, showing that a 2.5 pN force from a cell is exerted on a leg. The work performed in this step was 16-30% of the free energy of the hydrolysis of ATP molecules, suggesting that this step is linked to the elementary process of *M. pneumoniae* gliding. We discuss a model to explain the gliding mechanism, based on the information currently available.

Keywords: motility, optical tweezers, class *Mollicutes*, infection, sialic acid

OPEN ACCESS

Edited by:
Chih-Horng Kuo, Academia Sinica, Taiwan

Reviewed by:
Masayoshi Nishiyama, Kindai University, Japan
Ramanujam Srinivasan, National Institute of Science Education and Research (NISER), India

****Correspondence:***
Makoto Miyata
miyata@osaka-cu.ac.jp

†Present address:
Masaki Mizutani, Bioproduction Research Institute, National Institute of Advanced Industrial Science and Technology (AIST), Tsukuba, Japan

Specialty section:
This article was submitted to Microbial Symbioses, a section of the journal Frontiers in Microbiology

Received: *27 July 2021*
Accepted: *24 August 2021*
Published: *24 September 2021*

Citation:
Mizutani M, Sasajima Y and Miyata M (2021) Force and Stepwise Movements of Gliding Motility in Human Pathogenic Bacterium Mycoplasma pneumoniae. Front. Microbiol. 12:747905. doi: 10.3389/fmicb.2021.747905

INTRODUCTION

Members of the bacterial class *Mollicutes*, which includes the genus *Mycoplasma*, are parasitic and occasionally commensal bacteria that are characterized by small cells and genomes and by the absence of a peptidoglycan layer (Razin et al., 1998; Razin and Hayflick, 2010). *Mycoplasma* species bind to host cell surfaces and exhibit gliding motility to spread the infectious area. Interestingly, *Mycoplasma* gliding does not involve flagella or pili and is completely unrelated to other bacterial motility systems or conventional motor proteins that are common in eukaryotic motility (Miyata et al., 2020). The gliding motility of *Mycoplasma* is divided into two types, *Mycoplasma pneumoniae* and *Mycoplasma mobile*, which share no homology in component proteins, indicating independent mechanisms (Miyata and Hamaguchi, 2016a,b).

Mycoplasma pneumoniae is a human pathogen that causes respiratory diseases, including bronchitis and atypical pneumonia (Saraya, 2017). *M. pneumoniae* cells bind to human epithelial surfaces through sialylated oligosaccharides (SOs), which are major structures of animal cell surfaces related to cell-cell recognition, and the binding targets of many pathogens and toxins (Nagai and Miyata, 2006; Varki, 2008; Kasai et al., 2013; Williams et al., 2018). The cells show unidirectional gliding motility at a speed of up to 1 μm/s on SO-coated glass surfaces (**Figure 1A**; Nakane and Miyata, 2009; Miyata and Hamaguchi, 2016a), which is known to be essential for their infection (Prince et al., 2014). The gliding machinery, called the "attachment organelle," is localized at a cell pole (Seto et al., 2001). The attachment organelle is divided into two parts: internal and surface structures. The internal structure is composed of an internal core complex and a surrounding translucent area. The internal core comprises three parts: a terminal button, paired plates, and a bowl complex from the front side of the cell (**Figure 1B**; Nakane et al., 2015; Kawamoto et al., 2016; Miyata and Hamaguchi, 2016a). The major surface structure, called "P1 adhesin complex" or "genitalium and pneumoniae cytoadhesin (GPCA)," is composed of P1 adhesin and P40/P90 proteins and aligned around the internal structure, which plays a dual role as the adhesin to bind to SOs and as the leg for gliding (**Figure 1B**; Nakane et al., 2011; Aparicio et al., 2018, 2020; Vizarraga et al., 2020, 2021). The model for gliding called the "Inchworm model" or "Double-spring hybrid ratchet model" is proposed, in which cells repeat the extensions and contractions of the attachment organelle based on the energy from ATP hydrolysis to enable smooth gliding (Miyata, 2008; Kawamoto et al., 2016; Seybert et al., 2018; Mizutani and Miyata, 2019). Generally, the mechanical characteristics and detailed analysis of movements are essential for creating and completing a detailed model for the motility mechanism (Schnitzer and Block, 1997; Veigel et al., 1999; Tanaka et al., 2002; Mallik et al., 2004; Sowa et al., 2005). However, to date, no information is available about the force for gliding.

In the present study, we measured the stall forces of the two strains and discuss the relationship between binding and force. Furthermore, we succeeded in detecting and measuring stepwise movements that are likely linked to the elementary process of the gliding reaction.

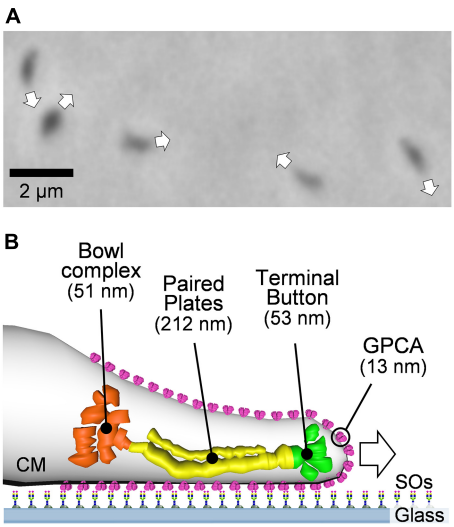

FIGURE 1 | Gliding motility of *Mycoplasma pneumoniae*. **(A)** Phase-contrast micrograph of *M. pneumoniae* cells. The gliding direction of cells are indicated by white arrows. **(B)** Illustration of gliding machinery. The gliding machinery is composed of bowl complex, paired plates, terminal button, and GPCA. The lengths along the cell axis were summarized from previous studies (Nakane et al., 2015; Vizarraga et al., 2020). GPCA, working as a leg is anchored to the cell membrane (CM) and catches sialylated oligosaccharides (SOs) fixed on solid surfaces.

MATERIALS AND METHODS

Strains and Cultivation

Mycoplasma pneumoniae M129 (ATCC29342) and FH strains were grown in SP-4 medium at 37°C in tissue culture flasks (TPP Techno Plastic Products AG, Trasadingen, Switzerland), as described previously (Tully, 1983; Nakane and Miyata, 2009). The FH strain was kindly provided by Tsuyoshi Kenri at the National Institute of Infectious Diseases, Tokyo, Japan.

Optical Tweezers System

An inverted microscope (IX71; Olympus, Tokyo, Japan) was equipped with a Nd:YAG laser (ASF1JE01; Furukawa Electric, Tokyo, Japan) to construct the optical tweezers. The microscope stage was replaced by a piezoelectric stage controlled by a stage controller (MDR14-CA-2.5; SIGMAKOKI, Tokyo, Japan) and a joystick (JS-300; SIGMAKOKI). The irradiated laser beam was concentrated as a finite optical system using a plano-convex lens supported by "optical cage system" (SIGMAKOKI). The concentrated laser beam was inserted into the microscope and focused by an objective lens (CFI Apochromat TIRF 100XC Oil; Nikon, Tokyo, Japan). The actual laser power was measured using a power meter (FieldMaxII; COHERENT, Santa Clara, CA, United States) without the objective lens.

Force Measurements

The cell suspension was mixed with 0.5 mM Sulfo-NHS-LC-LC-biotin (Thermo Fisher Scientific, Waltham, MA, United States) as the final concentration and incubated for 15 min at room temperature (RT). The cell suspension was centrifuged at 12,000 × *g* for 10 min, washed with 10 mM HEPES buffer (pH 7.4) containing 150 mM NaCl, centrifuged again, washed with HEPES buffer containing 10% non-heat-inactivated horse serum (Gibco; Thermo Fisher Scientific) and 20 mM glucose, passed through a 0.45-μm pore size filter and incubated for 15 min at RT. The cell suspension was inserted into a tunnel chamber, which was assembled by taping coverslips cleaned with saturated ethanolic KOH and precoated with 100% non-heat-inactivated horse serum for 60 min and 10 mg/ml bovine serum albumin (Sigma-Aldrich, St. Louis, MO, United States) in HEPES buffer for 60 min at RT. The tunnel chamber was washed with HEPES buffer containing 20 mM glucose and

incubated at 37°C on optical tweezers equipped with a thermo plate (MATS-OTOR-MV; Tokai Hit, Shizuoka, Japan) and a lens heater (MATS-LH; Tokai Hit). Avidin-conjugated beads in the HEPES buffer containing 20 mM glucose and 0.2-0.3 mM of 3′-*N*-acetylneuraminyllactose (SL) were sonicated and inserted into the tunnel chamber. The avidin-conjugated beads were prepared as previously described (Mizutani and Miyata, 2017). The bead movements were recorded using a charge-coupled device (CCD) camera (LRH2500XE-1; DigiMo, Tokyo, Japan) at 30 frames per second and analyzed by displacement of up to 200 nm from the trap center (the linear range of the laser trap) using ImageJ 1.43u[1] and IGOR Pro 6.33 J and 8.02 J (WaveMetrics, Portland, OR, United States) (Tanaka et al., 2016; Mizutani and Miyata, 2017; Mizutani et al., 2018). Measurements were performed using at least five individual cultures.

Binding and Gliding Analyses

Cultured cells were washed with buffer in a culture flask, and then washed with HEPES buffer containing 10% non-heat-inactivated horse serum (Gibco; Thermo Fisher Scientific) and 20 mM glucose. Cultured cells were scraped off the culture flask, passed through a 0.45-μm pore size filter, and incubated for 15 min at RT. The cell suspension was then inserted into the tunnel chamber. The tunnel chamber was washed with HEPES buffer containing 20 mM glucose, incubated at 37°C on an inverted microscope (IX83; Olympus) equipped with a thermo plate and lens heater, observed by phase-contrast microscopy at 37°C, and recorded with a CCD camera (DMK 33UX174; The Imaging Source Asia Co., Ltd., Taipei City, Taiwan). Then, the tunnel chamber was washed with HEPES buffer containing 20 mM glucose and various concentrations of SL. Video data were analyzed using ImageJ 1.43u and IGOR Pro 6.33 J. Measurements were performed using at least three individual cultures.

Genome Sequencing and Variant Analyses

Frozen stocks of cells were plated on Aluotto medium and isolated as previously described (Tulum et al., 2014). Genomic DNA was isolated and sequenced using MiSeq (Illumina, San Diego, CA, United States), as previously described (Mizutani et al., 2018). Sequence read mapping and variant detection were performed using the CLC Genomics Workbench (QIAGEN, Hilden, Germany).

RESULTS

Differences in Amino Acid Sequences of Gliding Proteins Between Two Strains

In this study, mainly we focused on a type strain "M129-B7," and also another major strain called "FH." The FH strain used in this study has not been genomically analyzed. Therefore, we sequenced the genomes of both strains using MiSeq (**Supplementary Data Sheet 1**) and analyzed the sequences of 14 genes that have been reported to be involved in binding and gliding (Miyata and Hamaguchi, 2016a). Only one amino acid was substituted in the M129 strain genome from the M129-B7 genome (GenBank accession no. CP003913), which was V196A in the HMW3 protein, which is positioned at the terminal button in the attachment organelle (**Figure 1B**). Our FH strain had 161 and 155 variations from the reported FH and FH2009 strains, respectively (GenBank accession no. CP010546 and CP017327), indicating that the FH strain is distant from the genome strains. The differences between the two strains analyzed in the present study in terms of the 14 genes were as follows: (i) P1 adhesin showed many differences, including 87 single amino acid substitutions, 18 amino acid insertions, and four amino acid deletions, known differences of FH from M129 strains (**Supplementary Figure 1**). (ii) The P40/P90 protein showed 96 single amino acid substitutions, one amino acid insertion, and 68 amino acid deletions (**Supplementary Figure 2**). (iii) The other 12 genes showed 0-5 mutations in each gene, as summarized in **Supplementary Table 1**.

Stall Force Measurement Using Optical Tweezers

Optical tweezers are commonly used to measure the stall force generated by pili in bacterial motility or motor proteins in eukaryotic motility (Kojima et al., 1997; Merz et al., 2000; Takagi et al., 2006; Gennerich et al., 2007). The stall force is defined as the force needed to stop movements and is equal to the maximal propulsion force for locomotion. Previously, we measured the stall force for the gliding motility of *M. mobile*, based on a mechanism unrelated to *M. pneumoniae* gliding, using optical tweezers (Miyata et al., 2002; Mizutani et al., 2018). In the present study, we applied this method to *M. pneumoniae* gliding. *M. pneumoniae* cells were biotinylated and inserted into a tunnel chamber, which was assembled using two glass plates and double-sided tape (Mizutani and Miyata, 2017). An avidin-conjugated polystyrene bead was trapped by a highly focused laser beam and attached to a gliding cell at the back end of the cell body by exploiting the avidin-biotin interaction. The cells pulled the bead from the trap center with gliding and then stalled (**Figures 2A,B** and **Supplementary Video 1**). The force was calculated by measuring the distance between the centers of the bead and the laser trap, which was multiplied by the trap stiffness; the force acting on the bead increased linearly with the displacement from the trap center (Kojima et al., 1997). Starting from 0 s, the pulling force increased and reached a plateau in 120 s (**Figure 2C**). The maximal value of the force averaged over 1 s was determined as the stall force. The stall force of M129 strain cells was 23.7 ± 6.3 pN (**Figure 2E**). We also measured the stall force of the FH strain. The cells of the FH strain pulled the bead in a manner similar to that of M129 cells (**Supplementary Video 2**). The stall force of the FH strain was 19.7 ± 5.3 pN, significantly weaker than that of the M129 strain (**Figures 2D,E**).

[1] http://rsb.info.nih.gov/ij/

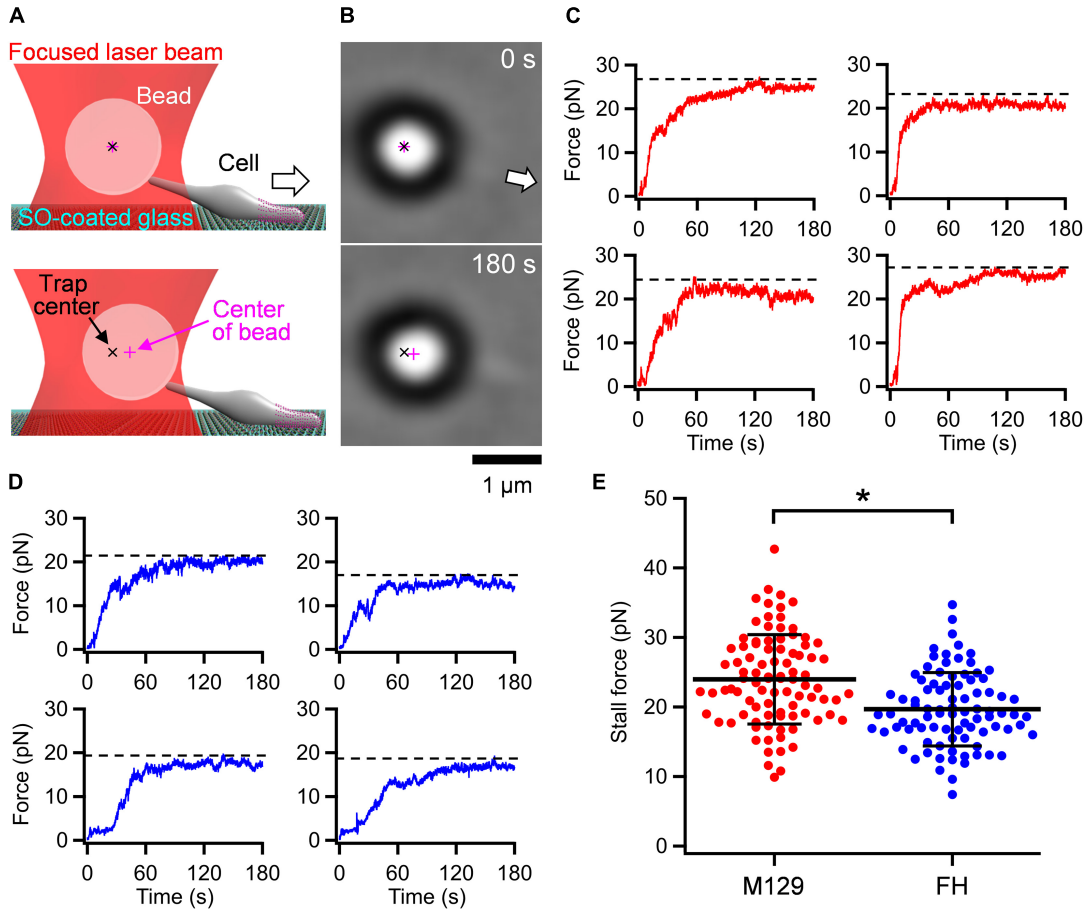

FIGURE 2 | Stall force measurements. **(A)** Illustrations of experimental design for force measurements. The white arrow indicates the gliding direction. **(B)** Optical micrographs of trapped cell. The cell attached with a bead (large black ring with white center) glided in the direction of white arrow from 0 and stalled in 180 s. The cell image can be observed near the base of arrow. **(C)** Four representative time courses of force increments for M129 strain. The broken lines indicate the values of stall force. **(D)** Four representative time courses of force increments for FH strain. The broken lines indicate the values of stall force. **(E)** Scatter dot plot of stall force (n = 92 and 88 in M129 and FH, respectively) shown with averages (thick lines) and standard deviations (thin lines). *$p = 2.4 \times 10^{-6}$ by Student's t-test.

Effect of Free Sialyllactose on Binding and Gliding

Mycoplasma pneumoniae cells have hundreds of legs and glide smoothly on solid surfaces. To trace the behavior of a single propulsion event, the number of working legs should be reduced by adding a free form of SO, which is the binding target for gliding (Kasai et al., 2013; Kinosita et al., 2014; Mizutani et al., 2018). To quantitatively analyze the effects of free SO on the binding activity and gliding under our conditions, we measured the bound ratio of cells and the gliding speed of the M129 strain under various concentrations of the SO, 3′-*N*-acetylneuraminyllactose (SL). *M. pneumoniae* cells suspended in the buffer were inserted into a tunnel chamber. Then, the cell behavior in 0–0.5 mM SL solutions was analyzed. The addition of free SL slowed down and then stopped gliding or released the gliding cells from the glass surfaces, but did not release non-gliding cells, indicating that release requires glass binding by GPCA with displacements (**Figure 3A**). The number of gliding cells and the gliding speed relative to the initial speed were decreased by 0.1-0.5 mM with SL treatments from 55 ± 11% to 26 ± 16% and from 0.33 ± 0.06 to 0.19 ± 0.07 μm/s, respectively (**Figures 3B,C**). We then decided to use 0.2-0.3 mM concentrations for further experiments because the binding and gliding were partially inhibited under these conditions, which were advantageous for observing single propulsion events caused by a single leg during gliding.

Stepwise Gliding Movements Observed Under Free SL

Next, we traced cells under 0.2-0.3 mM free SL conditions as performed in the stall force measurements. The gliding cells slowly pulled the beads from the trap center. Half of the tested cells stalled in 120 s, but the other cells repeated creeping movements and detachment from the glass surfaces (**Figure 4A**). The stall force of the cells that reached a plateau in 120 s was 16.2 ± 4.5 pN (**Figure 4B**), which was significantly weaker than that without SL ($p = 1.1 \times 10^{-5}$ by Student's t-test). In creeping movements, cells occasionally showed discontinuous

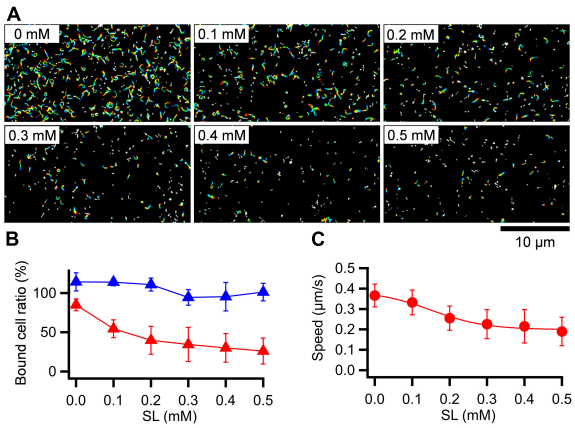

FIGURE 3 | Effects of SL on binding and gliding. **(A)** Gliding cells were treated with free SL. The cell trajectories after SL treatment are presented as a stack for 20 s, changing color from red to blue. SL concentrations are shown at left upper of each panel. **(B)** Number of cells bound to the glass at 5 min after the treatment are plotted relative to the initial cell number. The averages for gliding (red triangles) and non-gliding (blue triangles) cells are shown with the standard deviations (n = 10, 10, 10, 10, 9, 10 for 0, 0.1, 0.2, 0.3, 0.4, 0.5 mM, respectively). **(C)** Averaged gliding speeds under various SL concentrations are plotted with the standard deviations and fitted by a sigmoidal curve (n = 50, 50, 50, 50, 56, 56 for 0, 0.1, 0.2, 0.3, 0.4, 0.5 mM, respectively).

displacements, which were mostly stepwise (**Figures 4C,D**). Individual displacements in a stepwise time course were analyzed using the pairwise distance function (Kinosita et al., 2014; Mizutani et al., 2018). The displacements shown in **Figure 4D** were uniformly distributed at about 17-, 14-, and 16-nm intervals under 0.15, 0.20, and 0.17 pN/nm of trap stiffness, corresponding to 2.55, 2.80, and 2.66 pN of propulsion force, respectively (**Figures 4D,E**). Note that force increments are generally calculated from the trap stiffness × displacement (Kojima et al., 1997; Mizutani et al., 2018).

Next, to examine the load dependency of step sizes in detail, we measured step sizes under 0.07–0.26 pN/nm of trap stiffness. Ninety-seven steps in 36 cell trajectories, including at least two continuous steps, were detected. The step sizes under 0.13 to 0.26 pN/nm of trap stiffness linearly decreased from 21.0 to 8.0 nm with trap stiffness (**Figures 4F,H**). In contrast, the step sizes from 0.07 to 0.12 pN/nm of trap stiffness were mostly constant and distributed at 14-19 nm with an average of 16.2 ± 2.7 nm (n = 21) (**Figures 4G-I**).

From 0.07 to 0.12 pN/nm of trap stiffness, the force increments increased with the trap stiffness (**Figure 4I**). In the cases where the force values increase with trap stiffness, the calculated force does not reflect the actual force because the load is too small to influence the movements. Therefore, we focused on the force increments measured under 0.13–0.26 pN/nm of trap stiffness. The force exerted in a single propulsion step was concluded to be 2.5 ± 0.3 pN (n = 76) (**Figure 4J**).

Binding Activity and Gliding Motility

To discuss about the relationship between the binding activity and gliding speed, we analyzed them for the M129 and FH strains. *M. pneumoniae* cells were suspended in HEPES buffer containing 20 mM glucose to obtain an optical density at 595 nm of 0.07, then inserted into tunnel chambers. After incubation for 5–30 min, the tunnel chambers were washed and observed by phase-contrast microscopy. The number of bound cells in the M129 strain increased with time from 90 ± 16 to 308 ± 20 cells in 100 μm × 100 μm area from 5 to 30 min (**Figures 5A,B**). These values are consistent with the results of a previous report (Kasai et al., 2013). In contrast, the number of bound cells in the FH strain increased from 12 ± 2 to 36 ± 8 cells from 5 to 30 min (**Figures 5A,B**). The number of bound cells in the FH strain was 7.2-8.7-fold smaller than that of the M129 strain at all time points (**Figure 5B**). When 10 × concentrated cell suspension was examined, the bound cell numbers of the FH strain increased from 117 ± 10 to 386 ± 24 cells from 5 to 30 min, 1.2-1.3 times that of M129 at all time points (**Figures 5A,B**). These results indicate that the FH strain has approximately eightfold lower binding activity to SO-coated glass surfaces than the M129 strain. Considering that the stall force of FH was only 1.2-fold smaller than that of the M129 strain, the force is unlikely to be linked to binding activity.

Most of the bound cells showed gliding motility on the SO-coated glass (**Figure 5C** and **Supplementary Videos 3, 4**). To characterize gliding motility, the proportion of gliding cells and gliding speed were analyzed. The proportion of gliding cells to all bound cells was 78.1% (n_{total} = 2,284, n_{glide} = 1785) and 60.0% (n_{total} = 2,271, n_{glide} = 1,362) in the M129 and FH strains, respectively (**Figure 5C**). The gliding speeds averaged for 20 s at 1-s intervals were 0.47 ± 0.08 and 0.21 ± 0.07 μm/s for M129 and FH strains, respectively (**Figure 5D**). These results suggest that binding activity is not directly linked to gliding speed.

DISCUSSION

Mycoplasma pneumoniae Has Weak Stall Force

In the present study, we measured the stall force in *M. pneumoniae* gliding using optical tweezers. Previously, the stall force was measured for some bacterial surface motilities. *Neisseria gonorrhoeae* and *Myxococcus xanthus* show surface motility driven by the retraction of type IV pili (Pelicic, 2008). The stall forces of single-pilus retraction in *N. gonorrhoeae* and *M. xanthus* were measured by optical tweezers to be approximately 80 and 150 pN, respectively (Merz et al., 2000; Clausen et al., 2009). *M. mobile* glides up to 4.0 μm/s by a mechanism unrelated to that of *M. pneumoniae*. Previously, we measured the stall force of *M. mobile* gliding using optical tweezers to be approximately 113 pN (Mizutani et al., 2018). The stall forces of *M. pneumoniae* gliding were 23.7 ± 6.3 and 19.7 ± 5.3 pN in M129 and FH strains, respectively (**Figure 2E**), much weaker than those of other bacterial surface motilities. *M. pneumoniae* has a streamlined cell body about 0.2 μm in diameter (Hatchel and Balish, 2008). This shape and cell size may be beneficial for gliding in human tissues with weak forces.

In liquid culture, *M. pneumoniae* cells bind to the bottom surface of the tissue culture flask. This is distinct from the

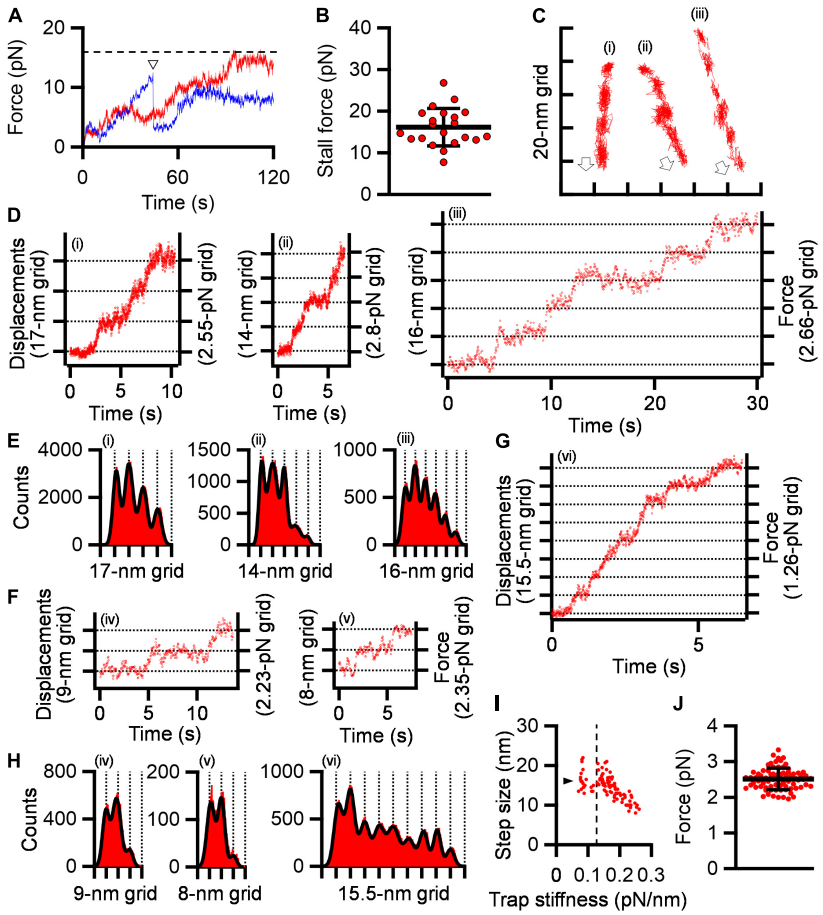

FIGURE 4 | Stepwise movements under SL. **(A)** Representative force traces with time under 0.2–0.3 mM SL are shown for stalled (red) and detached (blue) cells. The broken line indicates the stall force. The time point of detachment was marked by a triangle. **(B)** Scatter dot plot of stall force shown with averages (thick line) and standard deviations (thin lines) (n = 21). **(C)** Three cell trajectories with stepwise movements are shown in a field. Open arrows indicate the gliding direction. **(D)** Displacement and force of cells whose trajectories are shown in panel **(C)**. **(E)** Histograms of pairwise distance function (PDF) analysis of panel **(D)** were fitted by the sum of Gaussian curves. **(F)** Displacement and force under high trap stiffness. **(G)** Displacement and force under low trap stiffness. **(H)** Histograms of PDF analysis of panels **(F,G)**. **(I)** Distribution of step size under various trap stiffnesses. Step sizes were plotted as a function of trap stiffness (n = 97). The position at 0.12 pN/nm of trap stiffness was marked by a dotted line. The average of step size under 0.07–0.12 pN/nm of trap stiffness was marked by a triangle. **(J)** Scatter dot plot of force increments under 0.13–0.26 pN/nm of trap stiffness shown with averages (thick line) and standard deviations (thin lines) (n = 76).

case of *M. mobile*, in which most cells float in the medium. Therefore, *M. pneumoniae* is expected to have a stronger force for gliding than *M. mobile*. However, we found that *M. pneumoniae* had a much weaker stall force than *M. mobile* (**Figure 2E**). When comparing the two strains of *M. pneumoniae*, the FH strain showed much less active binding than, but a stall force comparable to, that of M129 (**Figures 2E, 3B**). These facts indicate that the binding activity of *M. pneumoniae* cells is not determined by the gliding force, which is represented by the stall force.

Drag Force in Gliding

The gliding speed decreased when cell binding was partially inhibited by the addition of free SL (**Figure 3**). This observation is consistent with previous data; that is, the inhibition of binding by monoclonal antibodies decreased the gliding speed of *M. pneumoniae* (Seto et al., 2005) and the inhibition by SL decreased the speed of *Mycoplasma gallisepticum*, coinciding with the common mechanism with *M. pneumoniae* (Mizutani and Miyata, 2019). The decrease in speed was probably caused by the drag force generated from the substrate surface, because the friction force exerted from water is estimated to be more than 5,000 times smaller than the stall force of 24 pN (**Figure 2E**; Rosengarten et al., 1988; Uenoyama et al., 2004). As the cause of the drag force, two possibilities are considered: GPCA and others. If some proportion of GPCA molecules are not involved in gliding, they are not released from SOs by inhibitory factors, resulting in speed reduction. Interestingly, these observations and explanations are similar to the case of *M. mobile* gliding, even though they do not share the same structure of machinery (Uenoyama et al., 2004, 2009; Kasai et al., 2013; Miyata and Hamaguchi, 2016b; Nishikawa et al., 2019). This scheme may be advantageous for gliding on SOs based on ATP energy, which is common in the both gliding mechanisms.

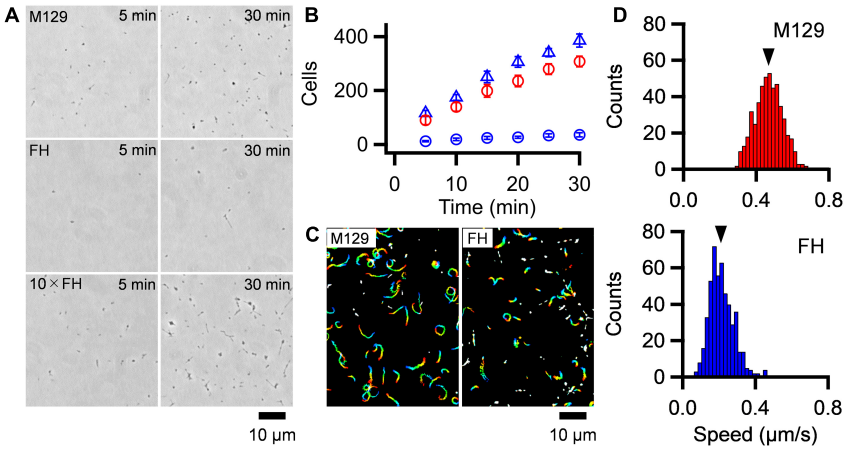

FIGURE 5 | Binding activity and gliding motility. **(A)** Phase-contrast micrographs of cells on SO-coated glass surfaces. M129, FH, and 10 × concentrated FH are shown after 5 and 30 min of incubations. **(B)** Averaged bound cell numbers in 100 μm × 100 μm plotted with standard deviations (n = 10 in each). M129 (Red open circle), FH (Blue open circle), and 10 × concentrated FH (Blue open triangle) are presented. **(C)** Cell trajectories for 20 s, changing color with time from red to blue. **(D)** Distributions of gliding speeds averaged for 20 s at 1-s intervals (n = 500 in each). The mean values are marked by black triangles.

Stepwise Movement as Elementary Process

We succeeded in detecting the stepwise movements of *M. pneumoniae* gliding. *M. pneumoniae* cells glided at a speed of 0.47 μm/s (**Figure 5D**), and the step size in the load-free condition was 14-19 nm (**Figure 4I**), suggesting 25-35 steps per second. The step size of *M. pneumoniae* is shorter than that of *M. mobile* around 70 nm (Kinosita et al., 2014, 2018; Mizutani et al., 2018). This difference is likely related to the lengths of leg complex, 13 nm in *M. pneumoniae* (Kenri et al., 2019; Aparicio et al., 2020; Vizarraga et al., 2021) and 97 nm in *M. mobile* (Miyata and Petersen, 2004; Adan-Kubo et al., 2006).

Stepwise movements are well-studied in ATP-driven eukaryotic motor proteins including myosin, dynein, and kinesin (Bustamante et al., 2004; Mallik et al., 2004). The force and displacement of a single step in myosin II, cytoplasmic dynein, kinesin-1, and myosin V have been reported as 3–5, 7–8, 8, and 2–3 pN and 5.3, 8, 8, and 36 nm, respectively (Kojima et al., 1997; Schnitzer and Block, 1997; Takagi et al., 2006; Gennerich et al., 2007; Fujita et al., 2012; Park and Lee, 2013). Stepwise movements are also present in bacterial motility. A flagellar motor shows 14 degrees of revolution as a step (Sowa et al., 2005; Nakamura et al., 2010). The gliding of *M. mobile* shows stepwise movements of 1.5 pN force and 70 nm length (Kinosita et al., 2014; Mizutani et al., 2018). Generally, stepwise movements are thought to correspond to the elementary process of a motility event.

Previously, we showed that *M. pneumoniae*-type gliding motility is driven by energy from ATP hydrolysis (Mizutani and Miyata, 2019). Motilities driven by ATP energy can be divided into elementary processes that are directly coupled with ATP hydrolysis, such as stepwise movements. The elementary processes observed as steps require a smaller amount of work than the energy produced by ATP hydrolysis, which is ∼80 pN nm (Yasuda et al., 1998). Therefore, we estimated the work done in the stepwise movements of *M. pneumoniae* gliding to determine this possibility. The work was estimated to be 18.2 ± 5.4 pN nm from the equation W_{step} = 0.5 × spring constant × displacement^2, under 0.13–0.26 pN/nm of trap stiffness, where the stiffness is large enough to determine the force (**Supplementary Figure 5**; Mizutani et al., 2018). This value is 16-30% of the free energy of the hydrolysis of ATP molecules, suggesting that we detected the elementary process of *M. pneumoniae* gliding. The energy conversion efficiencies of stepwise movements are 12-40, 10, and 40-60% for myosin II, cytoplasmic dynein, and kinesin, respectively (Bustamante et al., 2004; Mallik et al., 2004). Previously, we estimated it to be 10-40% for *M. mobile* gliding (Mizutani et al., 2018). These facts suggest that the energy efficiency of stepwise movements of *M. pneumoniae* is in a similar range of myosin II and *M. mobile* gliding, although we should be careful that here we measured a cell including many leg units, which is different from motor proteins even if we decreased the working numbers by adding SL.

Load-Dependent Step Size

M. pneumoniae cells showed different step sizes depending on the load provided by optical tweezers continuously (**Figure 4I**), suggesting that the step size of *M. pneumoniae* is load-dependent. In the infectious process, *M. pneumoniae* cells glide to the deep positions of respiratory systems and experience a large load at these positions (Prince et al., 2014). The load-dependent stepping behavior would be useful to glide against large loads because a load-independent stepping motor, kinesin, shows frequent back steps under large loads (Carter and Cross, 2006; Toleikis et al., 2020). Different step sizes under different loads have also been observed in *M. mobile* gliding (Kinosita et al., 2014; Mizutani et al., 2018).

Suggestion for Gliding Mechanism

How can we image the gliding mechanism? The GPCA probably plays a critical role in *M. pneumoniae* gliding, because antibodies

against the P1 adhesin, a component of GPCA, decreased the gliding speed and ultimately replaced the *M. pneumoniae* cells on the glass surface (Seto et al., 2005). Recently, the detailed structure of GPCA has been solved (Aparicio et al., 2018, 2020; Vizarraga et al., 2020, 2021). It is a mushroom structure composed of two P1 adhesins and two P40/P90 molecules. The C-terminal regions of the four molecules are bundled and anchored to the cell membrane. P40 and P90 proteins are synthesized as a single protein and processed into two proteins that are not observed in *M. genitalium*. Although P1 adhesin is believed to be the receptor for SOs, the binding site exists at the distal end of P40/P90. This complex is thought to undergo conformational changes between open and closed with respect to the binding pockets, which are likely involved in the gliding mechanism (Aparicio et al., 2020; Vizarraga et al., 2021).

The attachment organelle responsible for gliding can be divided into a surface structure including GPCA and an internal rod structure (Henderson and Jensen, 2006; Seybert et al., 2006, 2018; Kawamoto et al., 2016; Krause et al., 2018). Briefly, the force for gliding is likely generated at the bowl complex because a few proteins essential for gliding and not binding are localized there (Hasselbring et al., 2005; Jordan et al., 2007; Kawakita et al., 2016). The paired plates and elastic components play a role in force transmission, because the gliding speed decreases severely in a deletion mutant (Garcia-Morales et al., 2016). The terminal button likely connects the rod front to the cell membrane, because an end component, the P30 protein, features transmembrane segments (Chang et al., 2011; Relich and Balish, 2011).

Here, we focus on the following observations to construct the working model for the gliding scheme: (1) The force is probably generated around the bowl complex, transmits through the internal structures including paired plates, and reaches GPCAs. (2) Inhibition of cell binding decreases gliding speed. (3) GPCA has open and closed conformations. (4) Gliding can be divided into steps because binding and force are not tightly coupled. (5) The gliding movement can be divided into 14-19 nm steps with a 2.5 pN force.

Gliding Scheme to Explain Stepwise Movements

The model is composed of repeated cycle of four stages (i)-(iv) connected by four steps: "Power stroke," "Release," "Displacement," and "Catch" (**Figure 6**). (i) The GPCA in the open state catches an SO on the glass surface. (ii) Contraction of the internal structure pulls the cell body with 2.5 pN and a step size of 14-19 nm. This step is possibly linked to energy from an ATP molecule. (iii) GPCA switches into a closed state by triggering the pulling force transmitted from other working GPCAs, resulting in the release of after-stroke GPCA from the SO. (iv) The released GPCA returns to the open state and displaces another SO in the next position by the extension of the internal structure. (i) The GPCA captures the next SO. The full cycle was then repeated. This scheme explains the relationship between the binding and force of different strains, if we assume that release is enhanced and power stroke and catch are reduced in FH compared with those in M129, because force is determined by power stroke. The slow gliding speed in FH also can be explained by the reduction of catch step. These differences in the steps may be caused by the structural differences of the 14 proteins involved in binding and gliding. The characterization of defined genetic mutants may solve these problems. The observation that shorter steps occur under load can be explained if we consider that the power stroke is shortened by the load (**Figure 3I**).

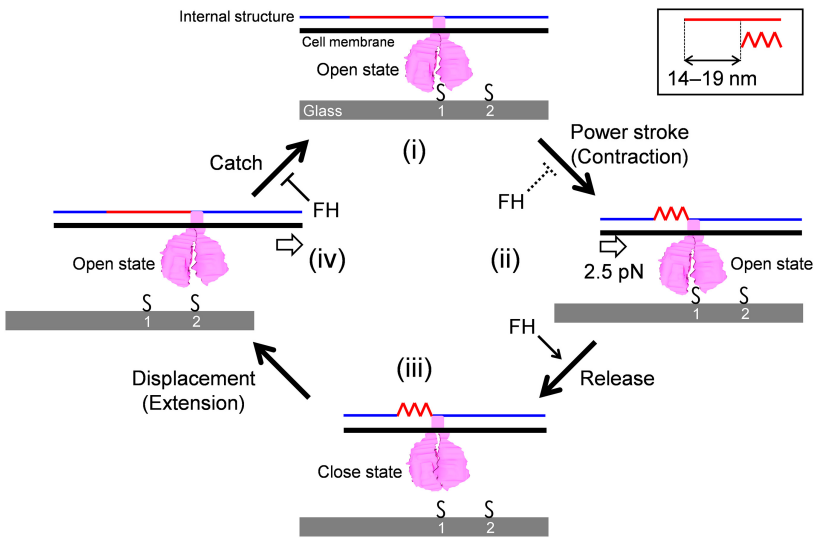

FIGURE 6 | Schematic illustration of leg behaviors in stepwise movements. Internal structure presented by blue and red lines is responsible for force transmission. It repeats contraction and extension cooperatively with the surface structures. Conformational change of internal structure and step size are shown in a right-upper box. GPCA is presented in pink. Sialylated oligosaccharides are shown by "S." Force exerted in a step is shown by an arrow in panel (ii). Displacement of cell body forward is shown by an arrow in panel (iv). The gliding occurs through stages (i)–(iv). See the text for details.

Previously, our group suggested a working model for *M. pneumoniae* gliding, focusing mainly on the information of the internal structure with regard to the attachment organelle (Kawamoto et al., 2016; Miyata and Hamaguchi, 2016a). The previous model suggested "directed detachment of feet" (GPCA), due to the lack of information about step, force, and foot structure. In this study, we succeeded in adding new information and completing an updated model.

DATA AVAILABILITY STATEMENT

The datasets presented in this study can be found in the **Supplementary Material**.

AUTHOR CONTRIBUTIONS

MMZ designed the study. MMZ and YS analyzed the genomes. MMZ performed all other experiments. MMZ and MMY wrote the manuscript, and all the authors completed it. All authors contributed to the article and approved the submitted version.

FUNDING

This work was supported by Grants-in-Aid for Scientific Research: (A) (MEXT KAKENHI Grant Number JP17H01544) and by JST CREST (Grant Number JPMJCR19S5, Japan). MMZ and YS are the recipients of a Research Fellowship of the Japan Society for the Promotion of Science (18J15362, 21J15218).

ACKNOWLEDGMENTS

We would like to thank Tsuyoshi Kenri at the National Institute of Infectious Diseases and Ikuko Fujiwara at Osaka City University for helpful discussions, and Shigeyuki Kakizawa at the National Institute of Advanced Industrial Science and Technology (AIST) for supporting the genome sequence analyses.

SUPPLEMENTARY MATERIAL

The Supplementary Material for this article can be found online at: https://www.frontiersin.org/articles/10.3389/fmicb.2021.747905/full#supplementary-material

Supplementary Figure 1 | Multiple sequence alignments for P1 adhesin of M129 and FH strains. The symbols "*" ":" "." indicate fully conserved residue, conservation between groups of strongly similar properties, and conservation between groups of weakly similar properties, respectively.

Supplementary Figure 2 | Multiple sequence alignments for P40/P90 of M129 and FH strains. The symbols "*" ":" "." indicate fully conserved residue, conservation between groups of strongly similar properties, and conservation between groups of weakly similar properties, respectively.

Supplementary Figure 3 | Work performed by stepwise movements. The scatter dot plot of works calculated from individual steps is shown with average (thick line) and standard deviation (thin lines).

Supplementary Table 1 | Amino acid variations of gliding related proteins in M129 and FH strains.

Supplementary Video 1 | Stall force measurement in M129 strain. A polystyrene bead was attached to the back end of cell body. The cell pulled the bead from trap center of optical tweezers. The video was played at 5 × speed.

Supplementary Video 2 | Stall force measurement in FH strain. A polystyrene bead was attached to the back end of cell body. The cell pulled the bead from trap center of optical tweezers. The video was played at 5 × speed.

Supplementary Video 3 | Gliding movement of M129 strain cells. Cells bound to the SO-coated glass surface were observed by phase-contrast microscopy. The video was played at 5 × speed.

Supplementary Video 4 | Gliding movement of FH strain cells. Cells bound to the SO-coated glass surface were observed by phase-contrast microscopy. The video was played at 5 × speed.

REFERENCES

Adan-Kubo, J., Uenoyama, A., Arata, T., and Miyata, M. (2006). Morphology of isolated Gli349, a leg protein responsible for *Mycoplasma mobile* gliding via glass binding, revealed by rotary shadowing electron microscopy. *J. Bacteriol.* 188, 2821–2828. doi: 10.1128/JB.188.8.2821-2828.2006

Aparicio, D., Scheffer, M. P., Marcos-Silva, M., Vizarraga, D., Sprankel, L., Ratera, M., et al. (2020). Structure and mechanism of the Nap adhesion complex from the human pathogen *Mycoplasma genitalium*. *Nat. Commun.* 11:2877. doi: 10.1038/s41467-020-16511-2

Aparicio, D., Torres-Puig, S., Ratera, M., Querol, E., Pinol, J., Pich, O. Q., et al. (2018). *Mycoplasma genitalium* adhesin P110 binds sialic-acid human receptors. *Nat. Commun.* 9:4471. doi: 10.1038/s41467-018-06963-y

Bustamante, C., Chemla, Y. R., Forde, N. R., and Izhaky, D. (2004). Mechanical processes in biochemistry. *Annu. Rev. Biochem.* 73, 705–748. doi: 10.1146/annurev.biochem.72.121801.161542

Carter, N. J., and Cross, R. A. (2006). Kinesin's moonwalk. *Curr. Opin. Cell Biol.* 18, 61–67. doi: 10.1016/j.ceb.2005.12.009

Chang, H. Y., Jordan, J. L., and Krause, D. C. (2011). Domain analysis of protein P30 in *Mycoplasma pneumoniae* cytadherence and gliding motility. *J. Bacteriol.* 193, 1726–1733. doi: 10.1128/JB.01228-10

Clausen, M., Jakovljevic, V., Sogaard-Andersen, L., and Maier, B. (2009). High-force generation is a conserved property of type IV pilus systems. *J. Bacteriol.* 191, 4633–4638. doi: 10.1128/JB.00396-09

Fujita, K., Iwaki, M., Iwane, A. H., Marcucci, L., and Yanagida, T. (2012). Switching of myosin-V motion between the lever-arm swing and brownian search-and-catch. *Nat. Commun.* 3:956. doi: 10.1038/ncomms1934

Garcia-Morales, L., Gonzalez-Gonzalez, L., Querol, E., and Pinol, J. (2016). A minimized motile machinery for *Mycoplasma genitalium*. *Mol. Microbiol.* 100, 125–138. doi: 10.1111/mmi.13305

Gennerich, A., Carter, A. P., Reck-Peterson, S. L., and Vale, R. D. (2007). Force-induced bidirectional stepping of cytoplasmic dynein. *Cell* 131, 952–965. doi: 10.1016/j.cell.2007.10.016

Hasselbring, B. M., Jordan, J. L., and Krause, D. C. (2005). Mutant analysis reveals a specific requirement for protein P30 in *Mycoplasma pneumoniae* gliding motility. *J. Bacteriol.* 187, 6281–6289. doi: 10.1128/JB.187.18.6281-6289.2005

Hatchel, J. M., and Balish, M. F. (2008). Attachment organelle ultrastructure correlates with phylogeny, not gliding motility properties, in *Mycoplasma pneumoniae* relatives. *Microbiology* 154, 286–295. doi: 10.1099/mic.0.2007/012765-0

Henderson, G. P., and Jensen, G. J. (2006). Three-dimensional structure of *Mycoplasma pneumoniae*'s attachment organelle and a model for its role in

gliding motility. *Mol. Microbiol*. 60, 376–385. doi: 10.1111/j.1365-2958.2006.05113.x

Jordan, J. L., Chang, H. Y., Balish, M. F., Holt, L. S., Bose, S. R., Hasselbring, B. M., et al. (2007). Protein P200 is dispensable for *Mycoplasma pneumoniae* hemadsorption but not gliding motility or colonization of differentiated bronchial epithelium. *Infect. Immun*. 75, 518–522. doi: 10.1128/IAI.01344-06

Kasai, T., Nakane, D., Ishida, H., Ando, H., Kiso, M., and Miyata, M. (2013). Role of binding in *Mycoplasma mobile* and *Mycoplasma pneumoniae* gliding analyzed through inhibition by synthesized sialylated compounds. *J. Bacteriol*. 195, 429–435. doi: 10.1128/JB.01141-12

Kawakita, Y., Kinoshita, M., Furukawa, Y., Tulum, I., Tahara, Y. O., Katayama, E., et al. (2016). Structural study of MPN387, an essential protein for gliding motility of a human-pathogenic bacterium, *Mycoplasma pneumoniae*. *J. Bacteriol*. 198, 2352–2359. doi: 10.1128/JB.00160-16

Kawamoto, A., Matsuo, L., Kato, T., Yamamoto, H., Namba, K., and Miyata, M. (2016). Periodicity in attachment organelle revealed by electron cryotomography suggests conformational changes in gliding mechanism of *Mycoplasma pneumoniae*. *MBio* 7, e00243–16. doi: 10.1128/mBio.00243-16

Kenri, T., Kawakita, Y., Kudo, H., Matsumoto, U., Mori, S., Furukawa, Y., et al. (2019). Production and characterization of recombinant P1 adhesin essential for adhesion, gliding, and antigenic variation in the human pathogenic bacterium, *Mycoplasma pneumoniae*. *Biochem. Biophys. Res. Commun*. 508, 1050–1055. doi: 10.1016/j.bbrc.2018.11.132

Kinosita, Y., Miyata, M., and Nishizaka, T. (2018). Linear motor driven-rotary motion of a membrane-permeabilized ghost in *Mycoplasma mobile*. *Sci. Rep*. 8:11513. doi: 10.1038/s41598-018-29875-9

Kinosita, Y., Nakane, D., Sugawa, M., Masaike, T., Mizutani, K., Miyata, M., et al. (2014). Unitary step of gliding machinery in *Mycoplasma mobile*. *Proc. Natl. Acad. Sci. U. S. A*. 111, 8601–8606. doi: 10.1073/pnas.1310355111

Kojima, H., Muto, E., Higuchi, H., and Yanagida, T. (1997). Mechanics of single kinesin molecules measured by optical trapping nanometry. *Biophys. J*. 73, 2012–2022. doi: 10.1016/S0006-3495(97)78231-6

Krause, D. C., Chen, S., Shi, J., Jensen, A. J., Sheppard, E. S., and Jensen, G. J. (2018). Electron cryotomography of *Mycoplasma pneumoniae* mutants correlates terminal organelle architectural features and function. *Mol. Microbiol*. 108, 306–318. doi: 10.1111/mmi.13937

Mallik, R., Carter, B. C., Lex, S. A., King, S. J., and Gross, S. P. (2004). Cytoplasmic dynein functions as a gear in response to load. *Nature* 427, 649–652. doi: 10.1038/nature02293

Merz, A. J., So, M., and Sheetz, M. P. (2000). Pilus retraction powers bacterial twitching motility. *Nature* 407, 98–102. doi: 10.1038/35024105

Miyata, M. (2008). Centipede and inchworm models to explain *Mycoplasma* gliding. *Trends Microbiol*. 16, 6–12. doi: 10.1016/j.tim.2007.11.002

Miyata, M., and Hamaguchi, T. (2016a). Integrated information and prospects for gliding mechanism of the pathogenic bacterium *Mycoplasma pneumoniae*. *Front. Microbiol*. 7:960. doi: 10.3389/fmicb.2016.00960

Miyata, M., and Hamaguchi, T. (2016b). Prospects for the gliding mechanism of *Mycoplasma mobile*. *Curr. Opin. Microbiol*. 29, 15–21. doi: 10.1016/j.mib.2015.08.010

Miyata, M., and Petersen, J. D. (2004). Spike structure at the interface between gliding *Mycoplasma mobile* cells and glass surfaces visualized by rapid-freeze-and-fracture electron microscopy. *J. Bacteriol*. 186, 4382–4386. doi: 10.1128/JB.186.13.4382-4386.2004

Miyata, M., Robinson, R. C., Uyeda, T. Q. P., Fukumori, Y., Fukushima, S. I., Haruta, S., et al. (2020). Tree of motility - A proposed history of motility systems in the tree of life. *Genes Cells* 25, 6–21. doi: 10.1111/gtc.12737

Miyata, M., Ryu, W. S., and Berg, H. C. (2002). Force and velocity of *Mycoplasma mobile* gliding. *J. Bacteriol*. 184, 1827–1831. doi: 10.1128/JB.184.7.1827-1831.2002

Mizutani, M., and Miyata, M. (2017). Force measurement on *Mycoplasma mobile* gliding using optical tweezers. *Bio Protoc*. 7:e2127. doi: 10.21769/BioProtoc.2127

Mizutani, M., and Miyata, M. (2019). Behaviors and energy source of *Mycoplasma gallisepticum* gliding. *J. Bacteriol*. 201, e00397–19. doi: 10.1128/JB.00397-19

Mizutani, M., Tulum, I., Kinosita, Y., Nishizaka, T., and Miyata, M. (2018). Detailed analyses of stall force generation in *Mycoplasma mobile* gliding. *Biophys. J*. 114, 1411–1419. doi: 10.1016/j.bpj.2018.01.029

Nagai, R., and Miyata, M. (2006). Gliding motility of *Mycoplasma mobile* can occur by repeated binding to *N*-acetylneuraminyllactose (sialyllactose) fixed on solid surfaces. *J. Bacteriol*. 188, 6469–6475. doi: 10.1128/JB.00754-06

Nakamura, S., Kami-Ike, N., Yokota, J. P., Minamino, T., and Namba, K. (2010). Evidence for symmetry in the elementary process of bidirectional torque generation by the bacterial flagellar motor. *Proc Natl Acad Sci U. S. A*. 107, 17616–17620. doi: 10.1073/pnas.1007448107

Nakane, D., Adan-Kubo, J., Kenri, T., and Miyata, M. (2011). Isolation and characterization of P1 adhesin, a leg protein of the gliding bacterium *Mycoplasma pneumoniae*. *J. Bacteriol*. 193, 715–722. doi: 10.1128/JB.00796-10

Nakane, D., Kenri, T., Matsuo, L., and Miyata, M. (2015). Systematic structural analyses of attachment organelle in *Mycoplasma pneumoniae*. *PLoS Pathog*. 11:e1005299. doi: 10.1371/journal.ppat.1005299

Nakane, D., and Miyata, M. (2009). Cytoskeletal asymmetrical dumbbell structure of a gliding mycoplasma, *Mycoplasma gallisepticum*, revealed by negative-staining electron microscopy. *J. Bacteriol*. 191, 3256–3264. doi: 10.1128/JB.01823-08

Nishikawa, M. S., Nakane, D., Toyonaga, T., Kawamoto, A., Kato, T., Namba, K., et al. (2019). Refined Mechanism of *Mycoplasma mobile* gliding based on structure, ATPase activity, and sialic acid binding of machinery. *MBio* 10, e02846–19. doi: 10.1128/mBio.02846-19

Park, P. J., and Lee, K. J. (2013). A modified active Brownian dynamics model using asymmetric energy conversion and its application to the molecular motor system. *J. Biol. Phys*. 39, 439–452. doi: 10.1007/s10867-013-9300-5

Pelicic, V. (2008). Type IV pili: *e pluribus unum*? *Mol. Microbiol*. 68, 827–837. doi: 10.1111/j.1365-2958.2008.06197.x

Prince, O. A., Krunkosky, T. M., and Krause, D. C. (2014). In vitro spatial and temporal analysis of *Mycoplasma pneumoniae* colonization of human airway epithelium. *Infect. Immun*. 82, 579–586. doi: 10.1128/IAI.01036-13

Razin, S., and Hayflick, L. (2010). Highlights of mycoplasma research–an historical perspective. *Biologicals* 38, 183–190. doi: 10.1016/j.biologicals.2009.11.008

Razin, S., Yogev, D., and Naot, Y. (1998). Molecular biology and pathogenicity of mycoplasmas. *Microbiol. Mol. Biol. Rev*. 62, 1094–1156. doi: 10.1128/MMBR.62.4.1094-1156.1998

Relich, R. F., and Balish, M. F. (2011). Insights into the function of *Mycoplasma pneumoniae* protein P30 from orthologous gene replacement. *Microbiology* 157, 2862–2870. doi: 10.1099/mic.0.052464-0

Rosengarten, R., Fischer, M., Kirchhoff, H., Kerlen, G., and Seack, K. H. (1988). Transport of erythrocytes by gliding cells of *Mycoplasma mobile* 163K. *Curr. Microbiol*. 16, 253–257. doi: 10.1007/BF01568687

Saraya, T. (2017). *Mycoplasma pneumoniae* infection: basics. *J. Gen. Fam. Med*. 18, 118–125. doi: 10.1002/jgf2.15

Schnitzer, M. J., and Block, S. M. (1997). Kinesin hydrolyses one ATP per 8-nm step. *Nature* 388, 386–390. doi: 10.1038/41111

Seto, S., Kenri, T., Tomiyama, T., and Miyata, M. (2005). Involvement of P1 adhesin in gliding motility of *Mycoplasma pneumoniae* as revealed by the inhibitory effects of antibody under optimized gliding conditions. *J. Bacteriol*. 187, 1875–1877. doi: 10.1128/JB.187.5.1875-1877.2005

Seto, S., Layh-Schmitt, G., Kenri, T., and Miyata, M. (2001). Visualization of the attachment organelle and cytadherence proteins of *Mycoplasma pneumoniae* by immunofluorescence microscopy. *J. Bacteriol*. 183, 1621–1630. doi: 10.1128/JB.183.5.1621-1630.2001

Seybert, A., Gonzalez-Gonzalez, L., Scheffer, M. P., Lluch-Senar, M., Mariscal, A. M., Querol, E., et al. (2018). Cryo-electron tomography analyses of terminal organelle mutants suggest the motility mechanism of *Mycoplasma genitalium*. *Mol. Microbiol*. 108, 319–329. doi: 10.1111/mmi.13938

Seybert, A., Herrmann, R., and Frangakis, A. S. (2006). Structural analysis of *Mycoplasma pneumoniae* by cryo-electron tomography. *J. Struct. Biol*. 156, 342–354. doi: 10.1016/j.jsb.2006.04.010

Sowa, Y., Rowe, A. D., Leake, M. C., Yakushi, T., Homma, M., Ishijima, A., et al. (2005). Direct observation of steps in rotation of the bacterial flagellar motor. *Nature* 437, 916–919. doi: 10.1038/nature04003

Takagi, Y., Homsher, E. E., Goldman, Y. E., and Shuman, H. (2006). Force generation in single conventional actomyosin complexes under high dynamic load. *Biophys. J*. 90, 1295–1307. doi: 10.1529/biophysj.105.068429

Tanaka, A., Nakane, D., Mizutani, M., Nishizaka, T., and Miyata, M. (2016). Directed binding of gliding bacterium, *Mycoplasma mobile*, shown by

detachment force and bond lifetime. *MBio* 7, e00455–16. doi: 10.1128/mBio.00455-16

Tanaka, H., Homma, K., Iwane, A. H., Katayama, E., Ikebe, R., Saito, J., et al. (2002). The motor domain determines the large step of myosin-V. *Nature* 415, 192–195. doi: 10.1038/415192a

Toleikis, A., Carter, N. J., and Cross, R. A. (2020). Backstepping mechanism of kinesin-1. *Biophys. J.* 119, 1984–1994. doi: 10.1016/j.bpj.2020.09.034

Tully, J. G. (1983). New laboratory techniques for isolation of *Mycoplasma pneumoniae*. *Yale J Biol. Med.* 56, 511–515.

Tulum, I., Yabe, M., Uenoyama, A., and Miyata, M. (2014). Localization of P42 and F_1-ATPase alpha-subunit homolog of the gliding machinery in *Mycoplasma mobile* revealed by newly developed gene manipulation and fluorescent protein tagging. *J. Bacteriol.* 196, 1815–1824. doi: 10.1128/JB.01418-13

Uenoyama, A., Kusumoto, A., and Miyata, M. (2004). Identification of a 349-kilodalton protein (Gli349) responsible for cytadherence and glass binding during gliding of *Mycoplasma mobile*. *J. Bacteriol.* 186, 1537–1545. doi: 10.1128/JB.186.5.1537-1545.2004

Uenoyama, A., Seto, S., Nakane, D., and Miyata, M. (2009). Regions on Gli349 and Gli521 protein molecules directly involved in movements of *Mycoplasma mobile* gliding machinery, suggested by use of inhibitory antibodies and mutants. *J. Bacteriol.* 191, 1982–1985. doi: 10.1128/JB.01012-08

Varki, A. (2008). Sialic acids in human health and disease. *Trends Mol. Med.* 14, 351–360. doi: 10.1016/j.molmed.2008.06.002

Veigel, C., Coluccio, L. M., Jontes, J. D., Sparrow, J. C., Milligan, R. A., and Molloy, J. E. (1999). The motor protein myosin-I produces its working stroke in two steps. *Nature* 398, 530–533. doi: 10.1038/19104

Vizarraga, D., Kawamoto, A., Matsumoto, U., Illanes, R., Perez-Luque, R., Martin, J., et al. (2020). Immunodominant proteins P1 and P40/P90 from human pathogen *Mycoplasma pneumoniae*. *Nat. Commun.* 11:5188. doi: 10.1038/s41467-020-18777-y

Vizarraga, D., Torres-Puig, S., Aparicio, D., and Pich, O. Q. (2021). The sialoglycan binding adhesins of *Mycoplasma genitalium* and *Mycoplasma pneumoniae*. *Trends Microbiol.* 29, 477–481. doi: 10.1016/j.tim.2021.01.011

Williams, C. R., Chen, L., Driver, A. D., Arnold, E. A., Sheppard, E. S., Locklin, J., et al. (2018). Sialylated receptor setting influences *Mycoplasma pneumoniae* attachment and gliding motility. *Mol. Microbiol.* 109, 735–744. doi: 10.1111/mmi.13997

Yasuda, R., Noji, H., Kinosita, K. Jr., and Yoshida, M. (1998). F_1-ATPase is a highly efficient molecular motor that rotates with discrete 120 degree steps. *Cell* 93, 1117–1124. doi: 10.1016/s0092-8674(00)81456-7

Conflict of Interest: The authors declare that the research was conducted in the absence of any commercial or financial relationships that could be construed as a potential conflict of interest.

Publisher's Note: All claims expressed in this article are solely those of the authors and do not necessarily represent those of their affiliated organizations, or those of the publisher, the editors and the reviewers. Any product that may be evaluated in this article, or claim that may be made by its manufacturer, is not guaranteed or endorsed by the publisher.

Copyright © 2021 Mizutani, Sasajima and Miyata. This is an open-access article distributed under the terms of the Creative Commons Attribution License (CC BY). The use, distribution or reproduction in other forums is permitted, provided the original author(s) and the copyright owner(s) are credited and that the original publication in this journal is cited, in accordance with accepted academic practice. No use, distribution or reproduction is permitted which does not comply with these terms.